THE JOURNAL OF PHYSICAL CHEMISTRY B

Article

pubs.acs.org/JPCB

α-Casein Inhibition Mechanism in Concanavalin A Aggregation Process

Rita Carrotta,* Silvia Vilasi, Fabio Librizzi, Vincenzo Martorana, Donatella Bulone, and Pier Luigi San Biagio

Institute of Biophysics, The National Research Council, Via Ugo La Malfa 153, 90146 Palermo, Italy

ABSTRACT: The inhibition of the aggregation in protein solutions is currently a subject of great interest in many research fields, from the study of protein-misfolding related diseases to pharmaceutics, biotechnology, and food science. α_{s1}-Casein, one of the four types of caseins, which are the largest protein component of bovine milk, has been found to hinder the aggregation process of several proteins, including the amyloid β-peptide, involved in Alzheimer's disease. To shed light into the mechanisms by which casein exerts this chaperon-like protective action, we studied its effect on the different steps of the aggregation process of concanavalin A, by means of both static and dynamic light scattering, thioflavin T and ANS fluorescence, circular dichroism, and atomic force microscopy. Our results show that casein has a poor effect on the first step of the process leading to the formation of amyloid-like structures. On the contrary, it has a marked effect on the second step of the process, ascribable to clusters condensation and compaction, up to the formation of very large aggregates. Such an effect requires a molar ratio of casein larger than that necessary to inhibit the fibrillogenesis of the amyloid β-peptide, thus, suggesting a different mechanism of interaction of casein, depending on both conformational properties and relative size of the aggregating molecules.

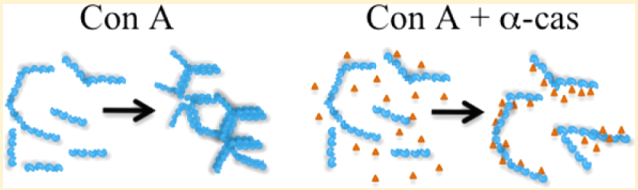

INTRODUCTION

The stabilization of proteins and the inhibition of their different aggregation processes are currently subjects of great interest in several research fields, from food science to biotechnology, and from pharmaceutical issues to protein-misfolding related diseases. Depending on parameters such as pH, ionic strength of the solvent, temperature and concentration, proteins may explore different regions of their conformational space and, thus, undergo different aggregation mechanisms and pathways.[1−4] As a result, different kinds of aggregates can be formed, going from amorphous to more ordered ones as crystals or β-rich structures like amyloid fibrils. As is well-known, many systemic amyloidoses are characterized by the presence of fibrillar protein deposits in the affected. The fibrillar aggregates play a role, not yet completely clear, in several neurodegenerative disorders such as Alzheimer's, Parkinson's, Creutzfeld-Jacob's, and Huntington's disease. Different proteins are implicated in these cases: Aβ-peptide, α-synuclein, prion protein, and huntingtin. It has been suggested that all proteins, although not involved in any kind of disease, may form amyloid aggregates when subjected to the proper, slightly destabilizing, conditions.[5−7] In fact, fibril formation is, in general, driven by mild stress conditions that allow metastable states to undergo intermolecular conformational rearrangements, reaching a more stable associated structure characterized by a deep free energy minimum. As a consequence, ordered aggregates are usually difficult to dissolve, even under strong treatments. Recently, great attention has been devoted to intermediate aggregates, large oligomers even formed by tens of monomers, which have been shown to be powerful toxins for cells.[8,9]

The inhibition of protein misfolding and of pathological protein aggregates formation is an extremely important subject. In vivo, these problems are faced by the cells through a system of recognition, refolding, or wasting, involving among other factors different molecular chaperones. Some of them are natively unfolded proteins that are able to interact with hydrophobic exposed patches, thus, recognizing wrong folding and avoiding aggregation. In vitro studies have reported the ability of HSPs (heat shock proteins) to interfere in the fibrillogenesis of huntingtin, α-synuclein, and Aβ-protein of the Dutch type and redirect the aggregation pathway toward the formation of more disordered, amorphous aggregates.[10,11] A similar inhibitory effect has been reported for α-casein (α-cas) in the aggregation process of several proteins (including the milk components α_{s2}-casein and κ-casein, able to form amyloid fibrils) and, importantly, in the fibrillogenesis of the Aβ-protein (Aβ).[12−15] This action is dose-dependent and is effective even at surprisingly low molar ratios, like Aβ/α-cas = 60:1. The understanding of the mechanisms by which α-cas, as well as HSPs, interferes with protein self-assembling mechanisms is clearly very important. The inhibitory effect has been related to some structural properties (high proline content, charged residues spread out distribution, very low intraresidues interaction), which are typical of the natively unfolded proteins and confer a very high flexibility to this class of proteins.[16−18] In this respect, it is worth noting that α_{s1}-casein, the main fraction

Received: July 26, 2012
Revised: November 6, 2012
Published: November 21, 2012

of α-cas, is a cysteine-free protein. In the case of the Aβ aggregation, α-cas may act by recruiting peptides, consistently having an effect on both the nucleation (delay) and growth phase (slowing down) of the process. A mechanism of colloidal inhibition, where α-cas colloidal particles interact with Aβ species (monomers/oligomers) has been proposed to explain these findings.[15,19] The mechanism is likely related to the relative mass ratio of the two monomeric components (4 and 24 KDa for Aβ-peptide and α-cas, respectively), the degree of unfolding and flexibility of both molecules, and the bridging effect characteristic of α-cas.[15] In fact, α-cas is usually modeled as a triblock copolymer constituted by two hydrophobic extreme portions and a central hydrophilic region.[15] New insights into the inhibition mechanisms of α-cas can be obtained by studying its effects on proteins of different size and properties and whose aggregation process displays different features. In this work we study the effect of α-cas on the aggregation process of concanavalin A (ConA), a folded protein, with a monomer mass of 26 KDa, comparable to that of the α-cas monomer. ConA is a bean agglutinin protein with a high tendency to aggregate.[20−24] Amyloid fibril formation has been detected at basic pH by atomic force microscopy (AFM) imaging and thioflavin T (ThT) fluorescence. In such conditions, the aggregation process is characterized by a three-step mechanism: protein conformational changes that probably lead to the formation of small aggregates with amyloid-like structure; fibril elongation and clusters condensation to form net-like aggregate structures; and compaction of the aggregate structure up to a fractal dimension close to 2.4.[24] These processes are differently intertwined when varying the concentration, affecting in this respect the overall apparent time course of the self-assembling. Circular dichroism (CD) and ThT emission signals very well correlate and probably indicate the formation at early times of β-structured aggregates. Surprisingly, this first process appears to be concentration-independent and is, therefore, rate limited by protein conformational changes, as is well evidenced by CD, ThT, and 1-anilinonaphthalene-8-sulfonic acid (ANS) emission changes. On the contrary, the subsequent condensation process strongly depends on protein concentration; at high concentration, it starts quite early and possibly overlaps with the first one.[24]

Our results show that α-cas only slightly affects the first conformational change limited process, as revealed by ThT, ANS, and CD signal. In contrast, the condensation process, monitored by means of static and dynamic light scattering, is significantly affected in a dose-dependent way by the presence of α-cas. The size and structure of the aggregates obtained with and without α-cas consistently appear very different, as is also confirmed by AFM imaging. All these results together suggest a mechanism by which α-cas clogs intermolecular hydrophobic regions of the ConA preformed β-structured aggregates, with a consequent delay and slowing down of clusters condensation and thickening.

EXPERIMENTAL METHODS

Sample Preparation. Lyophilized ConA (type IV, L7647), α-cas (α_s-casein with purity 70%, C6780), and ThT (T3516) were purchased from Sigma Aldrich and used without any further purification. All the measurements were performed in phosphate buffer, 0.1 M, pH 9. A fresh stock solution of α-cas was continuously stirred for 24 h in a cold room and passed through 0.22 μm filters. ConA solutions were freshly prepared at 6 °C, mixed when needed to α-cas at the proper ratio, and filtered directly into the suitable cuvette through 0.22 μm filters. ConA and α-cas concentration were separately determined by UV absorption at λ = 280 nm, using molar extinction coefficients of 33280 and 19116 cm^{-1} M^{-1}, respectively. ConA concentration ranged from 0.1 to 1.3 mg/mL. α-cas was mixed to ConA solutions at two different molar ratios ConA/α-cas, 1:1 and 4:1.

Static and Dynamic Light Scattering (SLS and DLS). Time-resolved light scattering experiments were carried on ConA/α-cas solutions, directly filtered in a quartz cylindrical cuvette, and incubated at T = 37 °C, in a thermostatically controlled cell compartment (0.1 °C tolerance). Measurements were performed on a Brookhaven Instrument BI200-SM goniometer, equipped with a 50 mW He−Ne laser with λ_0 = 632.8 nm. The intensity of the scattered light, $I(t)$, and its time autocorrelation function, $g_2(t)$, were measured simultaneously by using a Brookhaven BI-9000 correlator. Measurements were taken at the angle θ = 90°, corresponding to a scattering vector $q = (4\pi n/\lambda_0) \sin \theta/2 = 18.7$ μm^{-1}, where n is the refractive index of the solution and λ_0 is the in vacuo laser wavelength. The average intensity of the scattered light was monitored as a function of time in order to follow the growth of the weight-averaged mass, M_w, during the aggregation process of ConA, according to $M_w = (c_{ConA}M_{ConA} + c_{\alpha\text{-cas}}M_{\alpha\text{-cas}})/(c_{tot})$. In general, in the absence of direct interaction, $I_{90°}(t) \propto k[(c_{ConA}M_{ConA}P_{90°}(t)_{ConA}) + (c_{\alpha\text{-cas}}M_{\alpha\text{-cas}}P_{90°}(t)_{\alpha\text{-cas}})]$, with $k = ((4\pi^2n^2)/(\lambda^4N_A))(dn/dc)^2$, where n is the refractive index of the solution at T = 37 °C, N_A is the Avogadro number, and dn/dc is the derivative of n with respect to the protein concentration (we consider dn/dc = 0.18 cm^3/g^{-1}), $P_{90°}$ is the form factor, M is the protein molar mass, and c is the protein weight concentration. When the average size of the scattering particles is much smaller than the wavelength of the incident light ($d < \lambda_0/10$), $P_{90°} \simeq 1$ and the scattering intensity can be written $I_{90°}(t) \propto k[c_{ConA}M_{ConA} + c_{\alpha\text{-cas}}M_{\alpha\text{-cas}}] = kc_{tot}M_w$. Because this is the case at the beginning of the incubation, scattering data were normalized to $I_{90°}(0)$ in order to obtain the time course of the mass growth scaled to the initial weight averaged proteins mass. However, one must be aware that when large aggregates start to form, the scattering at 90° will be affected by the form factor of the aggregates. Actually, the latter can be used to study the structure of the protein aggregates. Thus, we performed measurements of the intensity of the scattered light at the end of the aggregation kinetics, as a function of the scattering vector, in the range 5−30 μm^{-1} (LALS, large angle light scattering), in order to obtain the structure factor $S(q)$ of the solution. The absolute scale for the scattered intensity was obtained by normalization with respect to toluene, whose Rayleigh ratio at 632.8 nm was taken as 14×10^{-6} cm^{-1}.

The intensity autocorrelation functions were analyzed by means of the cumulant analysis and a CONTIN-like[25] smoothing-constrained regularization method. In the former analysis, the intensity weighted z-averaged hydrodynamic radius R_h is calculated from the z-averaged diffusion coefficient D (obtained by the first cumulant coefficient) by assuming the Stokes−Einstein relation, $R_h = KT/6\pi\eta D$, where K is the Boltzmann constant, T is the absolute temperature, and η is the solvent viscosity. In the second analysis, the intensity weighted hydrodynamic size distribution is obtained by applying the Stokes−Einstein relation to the diffusion coefficients distribu-

dx.doi.org/10.1021/jp307417x | J. Phys. Chem. B 2012, 116, 14700−14707

tion, which is extracted by Laplace transformation of the field autocorrelation function.

Small Angle Light Scattering (SALS). For the samples of ConA at c = 1.3 mg/mL (without and with α-cas), time-resolved light scattering was also measured at q = 1.37 μm^{-1}. At the end of incubation the scattering was also measured as a function of the scattering wave vector q, in the range 0.02−2 μm^{-1}. A homemade experimental setup,[26] equipped with a 20 mW helium−neon laser and a charged coupled device Pulnix TM765 camera was used. Intensities can be measured over a wide dynamical range (from 1 to 33105 au) by means of a software integration of multiple exposure times (1/60 to 1/10000 s). SALS data are not in absolute scale and therefore to join LALS (see above) and SALS data, low q data were scaled to the high q ones by assuming that higher q SALS data lie on the straight line (on log−log scale) determined by fitting the low q LALS data. For the solution of ConA, the scaling was done to get coherent results at two different times (85 and 251 min) of incubation, while for the solution of ConA and α-cas, it was done on the final sample. The analysis of the structure factor data has been performed by assuming a fractal model for the aggregate. We used the expression[27]

$$S_m(q) = \frac{1}{m}\left[1 + \frac{d_f\Gamma(d_f - 1)\sin((d_f - 1)\arctan(q\xi))}{(qr_0)^{d_f}\left(1 + \frac{1}{q^2\xi^2}\right)^{(d_f-1)/2}}\right]$$

$$\text{for} \quad qr_0 \ll 1 \ll q\xi \qquad (1)$$

where m is the number of identical building units of radius r_0 in the aggregate (r_0 was fixed to 10 nm), Γ is the gamma function, ξ gives indication of the cluster size, and d_f is the fractal dimension, related to the structural packing of the fractal cluster. The function used is obtained analytically by assuming an exponential cutoff function, with the exponent ξ giving the size of the fractal aggregate. Late stage structure factors were fit by also considering a hard sphere interaction between the fractal clusters ($I(q) = S_m(q)\ S_{hs}(q,D/2,\Phi)$), whose fit parameters, $D/2$ and Φ, give the hard sphere radius and volume fraction, respectively.[27]

ThT and ANS Fluorescence. ConA amyloid aggregation was monitored in situ by measuring ThT and ANS fluorescence during the kinetic process. ThT or ANS were added to samples at the beginning of the process at a concentration of 50 μM. Both fluorophores did not change the aggregation process of ConA, as checked by monitoring time course turbidity from the aggregating solution, with and without the dye. Emission spectra were measured using a Jasco FP-6500 instrument, equipped with a cell holder thermostatted at T = 37 °C. Samples were filtered through 0.22 μm filters in a 1 cm path cuvette and emission spectra were recorded in the range 460−600 nm for ThT (λ_{ex} = 450 nm, 3 nm emission and excitation bandwidth, 100 nm/min scan speed, 2 s integration time) and 410−650 nm for ANS (λ_{ex} = 400 nm, 3 nm emission and excitation bandwidth, 200 nm/min scan speed, 1 s integration time). The increase of fluorescence was monitored at the band emission maximum (λ_{max} = 484 nm for ThT, λ_{max} = 474 nm for ANS). It was verified that ThT hydroxylation processes at basic pH does not affect the fibril detection.[28] It was also verified that a solution of 50 μM ThT/ANS and 1.1 mg/mL α-cas did not show any fluorescence increase during prolonged incubation at T = 37 °C.

Circular Dichroism (CD). The time evolution of the far-UV CD signal was recorded for ConA at 1.3 mg/mL, without and with α-cas, on a JASCO J-810 equipped with a Peltier unit for the temperature control. The CD signal at 215 nm was used to follow the conformational change kinetics during incubation at T = 37 °C. The CD spectra were measured using 50 nm/min as scan rate, 2 s of integration time, and a 0.2 mm optical path. As a reference, the spectrum of α-cas alone was also measured in the same experimental conditions.

AFM Measurements. ConA solution (1.3 mg/mL) without and with α-cas (ratio 1:1, monomer/monomer), incubated at 37 °C for about 1 day, was deposited on freshly cleaved mica and rinsed with superQ water. The samples were dried by a gentle nitrogen flux and imaged in air. AFM measurements were carried out in contact mode by using a homemade atomic force microscope with 38 μm scanning range. Cantilevers with silicon etched probe tips with a nominal spring constant of 0.15 N/m, 10 nm tip radius, 40° tip cone angle, and a resonance frequency of 12 kHz were purchased from Elbatech SRL. Images of 4 × 4 μm^2 in size were acquired in different regions of each sample at 1.5 Hz scan rate. Software for images analysis, WSxMv5.0, was developed by Nanotec Electronica.

RESULTS

Figure 1 reports the time course of the intensity scattered at q = 18.7 μm^{-1} at different concentrations of ConA, from 0.1 to 1.3 mg/mL. For each concentration, data relative to ConA alone and two different molar ratios of ConA/α-cas, 4:1 and 1:1, are reported. Because ConA is tetrameric in our experimental conditions, the two ratios correspond to one α-cas monomer for one tetramer of ConA and one monomer for monomer, respectively. Figure 1D also reports the scattered intensity for a sample of α-cas alone at the highest concentration used. As evident, α-cas does not aggregate in these experimental conditions, and therefore, the signal increase observed in the other samples must be entirely ascribed to ConA. The average molecular weight obtained for the sample

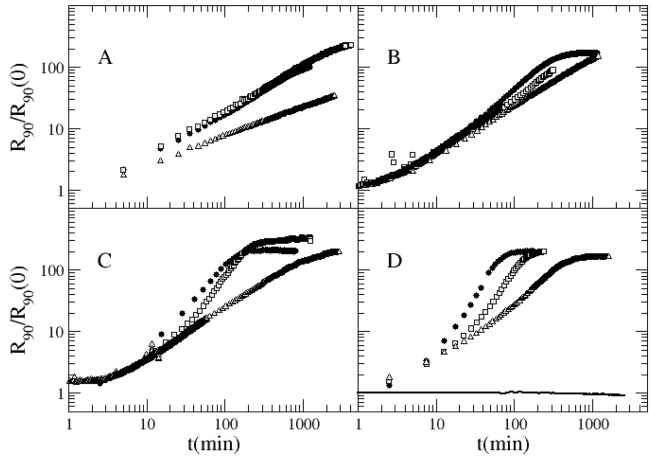

Figure 1. Raleigh ratio time course, normalized to the initial value at the beginning of incubation at T = 37 °C, for a solution of ConA (full circles) and ConA/α-cas at molar ratios 4:1 (squares) and 1:1 (triangles). ConA concentrations: 0.1 (A), 0.3 (B), 0.5 (C), and 1.3 mg/mL (D). (D) Time course of the scattered intensity for a sample of α-cas alone at the highest concentration used (1.2 mg/mL, continuous line).

dx.doi.org/10.1021/jp307417x | J. Phys. Chem. B 2012, 116, 14700−14707

of α-cas alone was about 120 KDa. Moreover, the analysis of dynamic scattering data by means of a CONTIN-based program[25] gave a size distribution characterized mainly by two species with dimensions of 10 and 100 nm, respectively (data not shown). These findings indicate that, besides the small species, ascribable to monomers and oligomers, the protein is also present, although in a very low extent, in some aggregated form. Although, in spanning α-cas concentration, we cross the so-called "micellar" critical value (0.14 mg/mL),[29,30] no discontinuity was noticed, in agreement with the evidence that the larger aggregate species (100 nm wide) were quite a negligible part of the sample. This suggests that the species exploiting the chaperone-like activity are the abundant monomer/oligomers, with dimensions of 10 nm.

Data relative to ConA/α-cas samples clearly show that α-cas slows down the aggregation process of ConA in a dose-dependent way; In fact, the effects on ConA aggregation are higher at higher α-cas concentration. Moreover, by keeping the same ConA/α-cas molar ratio, the effect is enhanced by increasing the ConA concentration (see Figure 1D). For the same samples, Figure 2 shows the evolution of the z-averaged

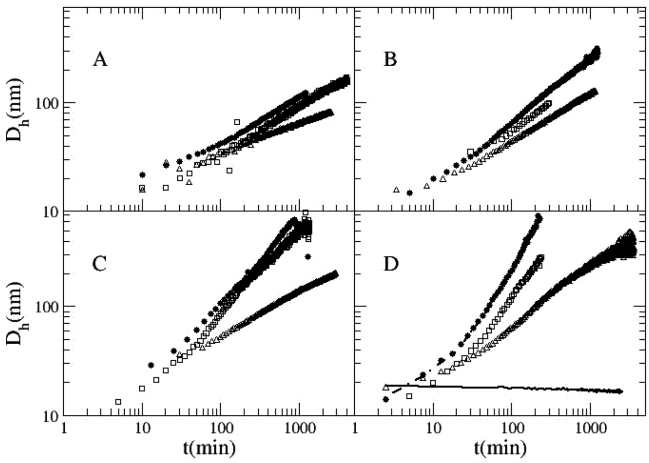

Figure 2. Time course of the average hydrodynamic diameter, obtained by cumulant analysis of the scattered intensity autocorrelation function, for solution of ConA (full circles) and ConA/α-cas at molar ratios 4:1 (squares) and 1:1 (triangles). ConA concentrations: 0.1 (A), 0.3 (B), 0.5 (C), and 1.3 mg/mL (D). (D) Average hydrodynamic diameter for a sample of α-cas alone at the highest concentration used (1.2 mg/mL, continuous line) and the calculated diameter by combining the results from ConA and α-cas alone, by assuming no interaction between the two (dash-dotted line).

hydrodynamic diameter, obtained by cumulant analysis. The comparison between Figure 1 and Figure 2 shows that, while the scattered intensity displays a saturation at long times, especially at high ConA concentration, the hydrodynamic radius still continues to grow. This indicates that the apparent saturation observed in Figure 1 must be considered as an effect of the aggregates form factor, which lowers the scattered intensity when the size of aggregates becomes comparable to the wavelength of the incident radiation. The aggregation process, however, keeps going on, as is clearly indicated by data in Figure 2. The average hydrodynamic diameter for a solution of α-cas alone, incubated under the same experimental conditions, is also reported in Figure 2D. As is evident, no increase is observed in the dimensions of α-cas, rather, a slightly decrease is observed, probably due to the dissolution of some aggregates.

In the limiting case of α-cas not participating in the ConA aggregation process, the average hydrodynamic diameter can be calculated from data relative to ConA alone and to α-cas alone according to $\langle D_h\rangle(t) = (I_{\alpha\text{-cas}} + I_{ConA}(t))/(I_{\alpha\text{-cas}}/D_{\alpha\text{-cas}} + I_{ConA}(t)/D_{ConA}(t))$. The obtained data (dash-dotted line in Figure 2D) are almost indistinguishable from those relative to ConA alone, and this clearly confirms the effect of α-cas on ConA aggregation process, on both mass (Figure 1) and hydrodynamic diameter (Figure 2) growths.

Figure 3 reports the field autocorrelation functions with their corresponding fitting curves (A) and the resulting size

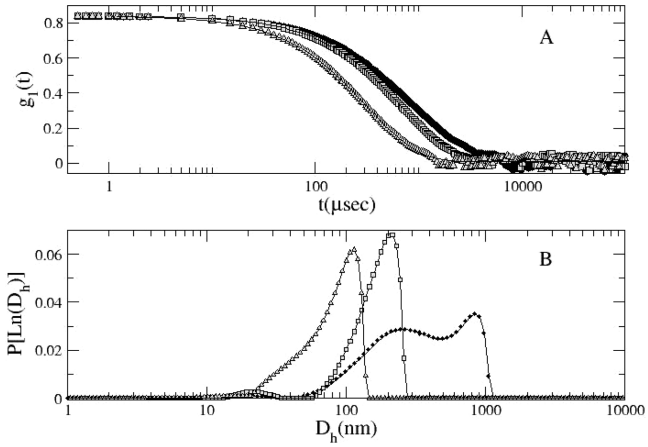

Figure 3. Field autocorrelation function data (A) measured after 100 min of incubation at T = 37 °C, for ConA at 1.3 mg/mL, with ConA/α-cas molar ratios 1:0 (full circles), 4:1 (gray squares), and 1:1 (gray triangles), respectively. Hydrodynamic diameter distributions (B) obtained by CONTIN-like analysis of the field autocorrelation data after 100 min of incubation.

distribution (B) for samples of ConA at 1.3 mg/mL concentration and different ConA/α-cas ratios. Data were taken at 100 min after the beginning of the process.

ConA aggregation has been described as the result of two intertwined processes: the first one, leading to β-aggregates formation, is accompanied and rate limited by protein conformational changes and does not show any rate dependence on protein concentration; the second one displays an evident concentration dependence of the growth rates and arises from clusters condensation, up to the formation of aggregates in the scale of tens of micrometer.[24] The first process, recognizable by the increase of ThT fluorescence, that is indicative of the formation of amyloid-like structures, has been found to correlate well with changes in far-UV circular dichroism and ANS fluorescence signals. These changes reach a plateau in about 100 min, no matter what is the ConA concentration. The signals, however, partially overlap with the aggregates growth brought about by the second process, which can be detected by light scattering and lasts for a time at least 1 order of magnitude longer. Figure 4 shows the time course of ThT and ANS emission maxima (A) and of the circular dichroism signal at 215 nm (B), for samples at high ConA concentration (1.0 mg/mL), without and with α-cas at 1:1 ratio (CD spectra at the beginning and the end of the kinetics are reported in Figure 5). For the sake of comparison, in Figure 4B also is reported the normalized scattering intensity growth for

dx.doi.org/10.1021/jp307417x | J. Phys. Chem. B 2012, 116, 14700−14707

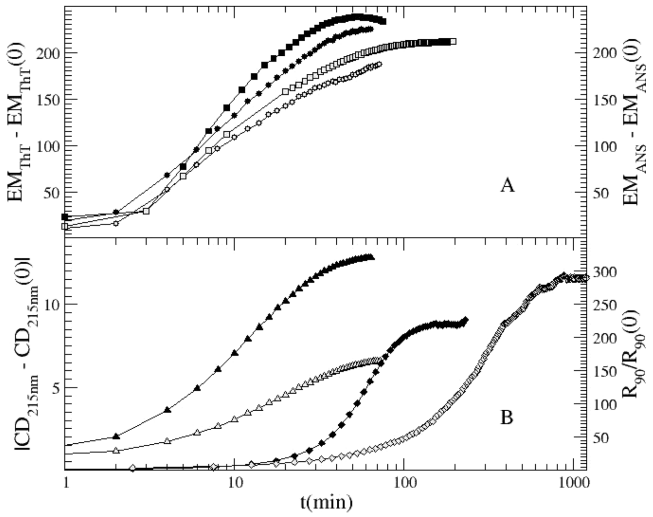

Figure 4. (A) Time course of thioflavin T (circle) and ANS (square) emission for ConA at 1 mg/mL, alone (full symbols) and with α-cas at a 1:1 molar ratio (gray symbols). (B) Time course of CD absolute value at λ = 215 nm (triangles, full and gray symbols for ConA alone and with α-cas at a 1:1 molar ratio, respectively) and the light scattering intensity monitored at q = 18.7 μm^{-1} for solutions of ConA at 1.3 mg/mL, alone (full diamond), and with α-cas at a molar ratio of 1:1 (gray diamond); data already reported in Figure 1D.

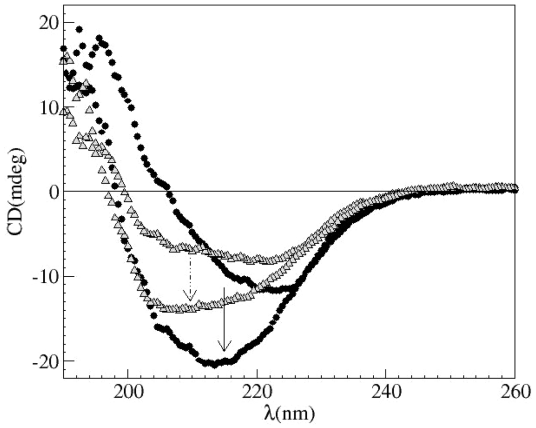

Figure 5. Far-UV CD spectra at the beginning and the end of incubation for solutions of ConA alone (full circles) and with α-cas (gray triangles). ConA concentration is 1 mg/mL and ConA/α-cas = 1:1. The arrows indicate the time direction.

the samples with c_{ConA} = 1.3 mg/mL, without and with α-cas at 1:1 molar ratio. Data in Figure 4 show that the presence of the α-cas affects, to some extent, even the preliminary formation of the "amyloid-like" structures at the conformational level, as especially detected by CD. ThT, as well as ANS binding, however, appear less sensitive to α-cas. In fact, while far-UV CD is mainly due to secondary structure conformational properties, ThT and ANS binding can be related also to structural changes on different scales involving tertiary structure changes. However, the characteristic times of the two signals are slightly affected by α-cas presence. Therefore, data reported in Figures 1−4 show that α-cas affects the two steps of the ConA aggregation process in a different way: there is only a partial effect on the first process, developing in less extent but with the same characteristic time, as detected by CD, ThT, and ANS fluorescence (Figure 4), while a sizable effect is observed on the following condensation process, as detected by light scattering (Figures 1−4).

All these results point to a model where α-cas molecules do not affect the early step of ConA β-aggregates formation. The process is likely characterized by some kind of specific interaction among ConA molecules and, therefore, appears not really influenced by α-cas, although CD results show that an interaction of α-cas/ConA cannot be ruled out. ANS data show that the first step leads to the formation of hydrophobic structures, which are responsible for the following colloidal condensation. At this point, α-cas likely acts on a different length scale than ANS molecules, by shielding such hydrophobic structures. The α-cas molecules (both interacting with ConA in the first association step or recognizing later the preformed aggregates) are able to interpose among the β-aggregates, being effective in slowing their further assembling, growth, and thickening. Due to the fact that these steps are strongly protein concentration dependent, the α-cas effect is enhanced at high concentration of ConA (Figures 1A−D and 2A−D).

The formation of large aggregate clusters on the scale of some micrometers during the second process has been further investigated by means of small angle light scattering, in a q range from 0.01 to 30 μm^{-1}. Figure 6A reports the growth of the intensity scattered at q = 1.37 and 18.7 μm^{-1}. Figure 6B reports the q dependence of the scattered intensity at the end of the incubation for samples at the highest concentration of ConA (1.3 mg/mL), without and with α-cas in the ratio 1:1. As is evident in Figure 6A, data obtained at low q, either in the presence or absence of α-cas, show a delay in the growth and in the final plateau with respect to those obtained at large q. This again confirms that the plateau in the intensity growth is not due to an arrest of the aggregation process, but to the effect of the form factor, which clearly affects in a different way the intensity measured at low and at high q. Data reported in Figure 6B have been analyzed by applying a fractal model to the average aggregate structure factor (eq 1). Two different species characterized by the same fractal dimension 2.4, with sizes of about 4 and 20 μm, respectively, are sufficient to describe data relative to ConA alone. A species of size 1.4 μm and lower fractal dimension 1.6, was found for the aggregates formed in the presence of α-cas. The mass fractal dimension can vary in the range 1−3, for objects having from linear to spherical mass distribution in the limit cases. Studies on protein structures lead to an average fractal dimension of 2.5, resulting from a filled space corresponding to 3/4 of the volume within the protein surface.[31] Therefore, a fractal dimension of 2.4 reflects a quite high compactness. On the other hand, the value 1.6 is close to that found for self-avoiding random coils[32] and linear elongated flexible aggregates.[33] In the present case, the lower value obtained for the mass fractal dimension of the aggregates formed in the presence of α-cas supports the hypothesis of the clogging of α-cas molecules on the ConA aggregates surface. This, in fact, likely brings to the concealment of those metastable regions in the clusters with a tendency to further interact. In both cases (without and with α-cas), a hard sphere interaction factor is also included in the fit expression, giving a volume fraction of interacting aggregates of 9.5 and 9.7% and a hard-sphere radius of 2.8 and 2.7 μm, for ConA alone and ConA with α-cas, respectively (Table 1 summarizes the parameters of the fitting curves). Figure 7 shows some representative AFM images of the two samples at the end of the kinetics. In accordance with light scattering data, the

dx.doi.org/10.1021/jp307417x | J. Phys. Chem. B 2012, 116, 14700−14707

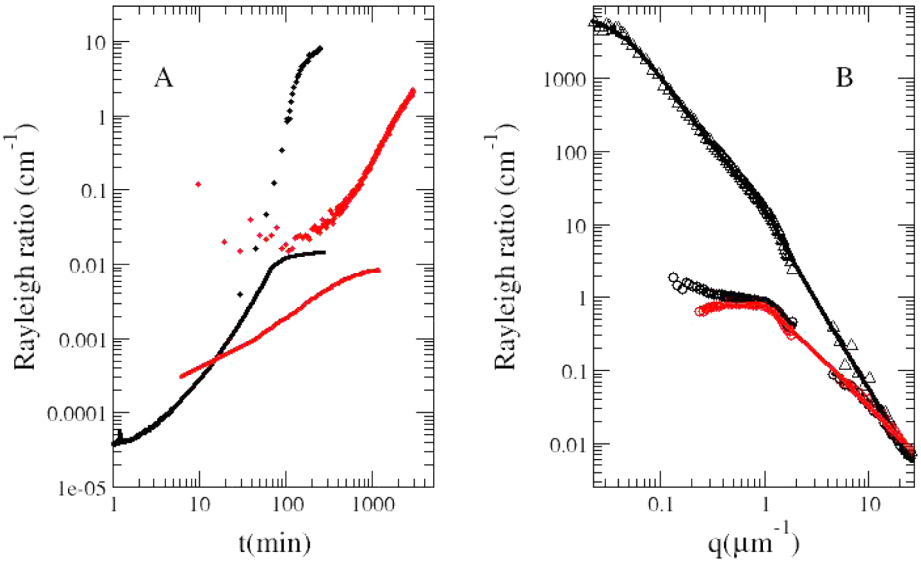

Figure 6. (A) In situ light scattering time course at two different q values, q = 1.37 μm^{-1} (symbols) and 18.7 μm^{-1} (lines), for a solution of ConA alone (black) and ConA/α-cas at molar ratios 1:1 (red). (B) Scattered intensity as a function of q for ConA alone at two different incubation times (85 min, black circles; 251 min, black triangles) and for ConA/α-cas at molar ratios 1:1 at the end of the monitored kinetics (1460 min, red circles). Data were obtained by combining multiangle light scattering (4−30 μm^{-1}) and small-angle light scattering (0.01−2 μm^{-1}). The continuous lines are the best fitting curves according to the fractal model described in the text. ConA concentration is 1.3 mg/mL.

Table 1. Parameters Resulting from the Fit According to the Fractal Model (Eq 1)

	ξ_1 (μm)	ξ_2 (μm)	d_f	Φ	$D/2$ (μm)
ConA	5 ± 1	20 ± 2	2.4 ± 0.1	0.095 ± 0.02	2.8 ± 0.1
ConA + α-cas	1.40 ± 0.05		1.6 ± 0.1	0.097 ± 0.02	2.7 ± 0.1

aggregates are smaller in the presence of α-cas and with a structure compatible with the smaller fractal dimension obtained by the analysis of the structure factor (Figure 6B and Table 1).

DISCUSSION AND CONCLUSIONS

ConA is here used as an aggregating protein model system to investigate the mechanisms by which α-cas affects and partially inhibits protein aggregation. ConA self-assembly at high pH has been described as a multistep aggregation process involving the formation of amyloid-like structures, further associating in clusters, which in turn grow in dimensions (up to tens of micrometers) and in compactness, as indicated by the fractal dimension. As recently reported, the latter phase can be modeled as a colloidal, concentration dependent, aggregation that apparently can be diffusion or reaction limited, depending on the concentration regime (low or high, respectively). The link between the preliminary concentration independent process leading to the formation of amyloid-like structures and the following colloidal aggregation probably plays a role in determining the concentration dependence of the overall process.[24]

Due to its ability in detecting aggregates ranging from nanometers to tens of micrometers, multiangle light scattering was used as the main technique to highlight α-cas effect on ConA aggregation. The results show that α-cas affects in a dose-dependent way the colloidal aggregation of ConA, which leads to clusters formation and thickening of the aggregates, while seems much less effective on the first step of the aggregation process, which, as recently reported,[24] is rate-limited by some kind of conformational rearrangement. Because the second step of aggregation is strongly concentration-dependent, α-cas effects are markedly evident at high concentration and barely noticeable at low concentration. The strong difference between the effect of α-cas on the first and second step of ConA aggregation suggests that α-cas accomplishes its action mainly in an unspecific way, by acting on the hydrophobic patches still present on β-aggregates. In fact, to affect the first process that leads to the formation of amyloid-like structures, α-cas would have required a very specific interaction with ConA tetramers. ANS and ThT fluorescence respond only to the first step of the aggregation process and therefore are not heavily affected by α-cas presence. Importantly, ANS data confirm that the first step of the aggregation leads to the formation of hydrophobic structures; α-cas recognizes and clogs these structures, probably on a larger scale than ANS, thus, bringing about a reduction of the hydrophobic interactions and a significant slowing down of the condensation process.

Recent studies have shown that α-cas acts on amyloid β-peptide (Aβ) aggregation through a mechanism of colloidal inhibition, where the peptide is sequestered, with an effective lowering of its free concentration. Aβ monomers are about 6-fold smaller than α-cas monomers. In this case, α-cas was found effective at very low molar ratios, like 60:1, thus indicating that α-cas "sequestering effect" strongly acts also on the intermediate prefibrillar unordered species, which in the absence of α-cas would trigger the cooperative fibrillogenesis mechanism.[15] In the case of ConA instead α-cas effect shows up at higher molar ratios. Probably, the difference in the extent of α-cas effects in Aβ peptide and ConA aggregation can be ascribed to the different mechanisms of interaction/inhibition, due to both the relative mass ratio and the different conformational properties of the proteins, Aβ peptide (unfolded) and ConA (globular tetramer, folded or partially

dx.doi.org/10.1021/jp307417x | J. Phys. Chem. B 2012, 116, 14700−14707

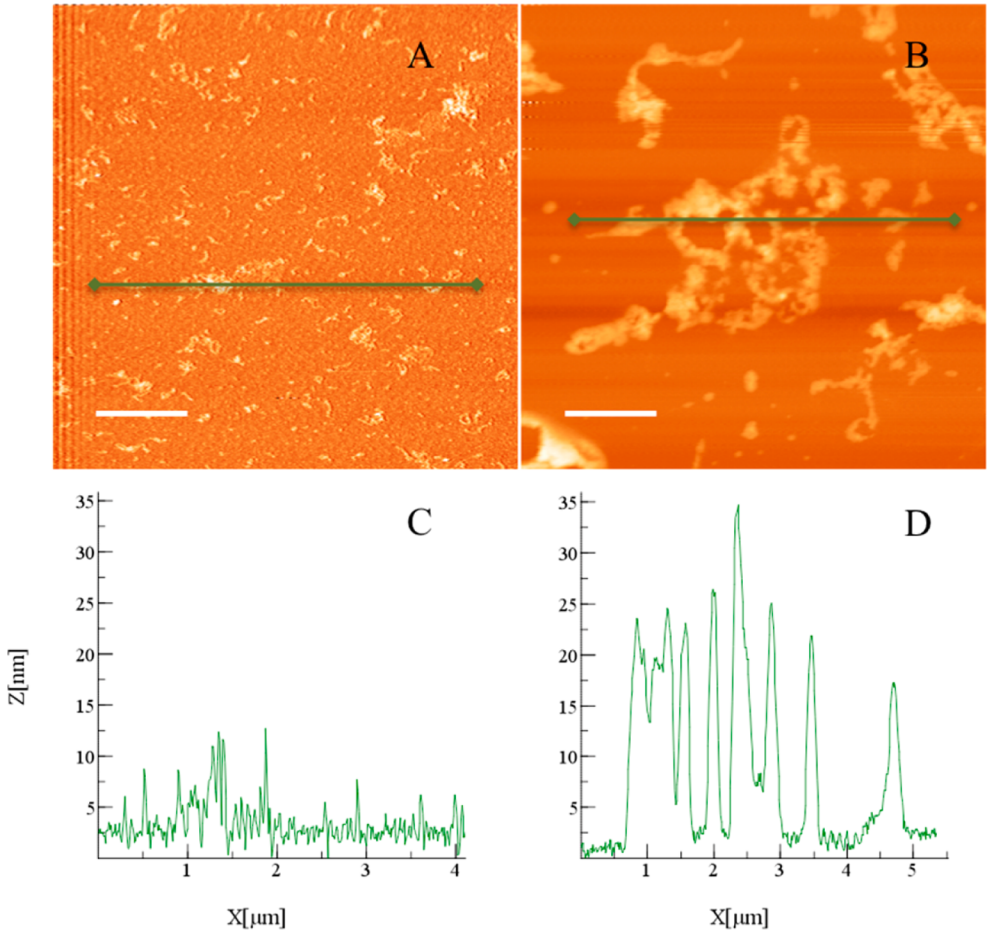

Figure 7. AFM representative images of two samples of ConA/α-cas at molar ratio 1:1 (A) and ConA alone (B), at the end of incubation at T = 37 °C; scale bars are 1 (A) and 1.3 μm (B). (C, D) Height profile relative to the sections indicated by the green lines in (A) and (B), respectively. ConA concentration is 1.3 mg/mL.

unfolded). In fact, similarly to what happens for other intrinsically disordered proteins (IDPs), Aβ peptide undergoes a chain collapse phenomenon that precedes the amyloid fibril formation.[34−36] The Aβ unstructured collapsed globule presents a conspicuous uninterrupted hydrophobic patch that covers 25% of the surface.[34] We can hypothesize that unordered chaperones, like α-cas, may exert their activity by means of a common mechanism that mainly involves the binding/shielding of exposed hydrophobic surfaces. These latter are present in the Aβ initial unstructured coil and characterize the patches involved in ConA cluster formation. An unspecific clogging mechanism inhibiting ConA aggregation is suggested in this latter case. The "hydrophobic" inhibition hypothesis would be at the basis of the role exerted in milk by α- and β-caseins in preventing fibril-forming propensity of k-casein, an IDP that adopts a collapsed form before amyloid aggregation.[13] In conclusion, chaperone-like activity of α-cas unravels through different mechanisms, depending on both conformational properties and relative size of the aggregating macromolecules. These results shed new light into the comprehension and usage of α-cas as a stabilizing agent, able to influence aggregation protein pathways, similar to heat-shock proteins.

AUTHOR INFORMATION

Corresponding Author

*E-mail: rita.carrotta@pa.ibf.cnr.it. Tel.: +39 091 6809313. Fax: +39 091 6809350.

Notes

The authors declare no competing financial interest.

ACKNOWLEDGMENTS

This work was partially supported by the Italian Ministry of University and Research (PRIN 'Sviluppo di una strategia molecolare per la prevenzione dell'aggregazione proteica e della fibrillogenesi: un approccio biofisico' and MERIT 'Basi molecolari nelle sindromi degenerative correlate con l'invecchiamento'). We thank Ing. F. D'Anca and M. Zora for the optimization of the AFM setup in the frame of Biojerker project. Technical support by A. Provenzano is also acknowledged.

REFERENCES

(1) Fink, A. L. *Fold. Des.* **1998**, *3*, R9−R23.
(2) Deyoung, L. R.; Fink, A. L.; Dill, K. A. *Acc. Chem. Res.* **1993**, *26*, 614−620.
(3) Piazza, R. *Curr. Opin. Colloid. Int. Sci.* **2000**, *5* (1−2), 38−43.
(4) Chiti, F.; van Nuland, N. A. J.; Taddei, N.; Margherini, F.; Ramponi, G.; Dobson, C. M. *Biochemistry* **1998**, *37* (5), 1447−1455.
(5) Dobson, C. M. *Trends Biochem. Sci.* **1999**, *24* (9), 329−332.

(6) Booth, D. R.; Sunde, M.; Bellotti, V.; Robinson, C. V.; Hutchinson, W. L.; Fraser, P. E.; Hawkins, P. N.; Dobson, C. M.; Radford, S. E.; Pepys, M. B. *Nature* **1997**, *385* (6619), 787−793.
(7) Chiti, F.; Webster, P.; Taddei, N.; Clark, A.; Stefani, M.; Ramponi, G.; Dobson, C. M. *Proc. Natl. Acad. Sci. U.S.A.* **1999**, *96* (7), 3590−3594.
(8) Lambert, M. P.; Barlow, A. K.; Chromy, B. A.; Freed, R.; Liosatos, M.; Morgan, T. E.; Rozovsky, I.; Trommer, B.; Viola, K. L.; Wals, P.; Zhang, C.; Finch, C. E.; Krafft, G. A.; Klein, W. L. *Proc. Natl. Acad. Sci. U.S.A.* **1998**, *95*, 6448−6453.
(9) Kokubo, H.; Kayed, R.; Glabe, C. G.; Yamaguchi, H. *Brain Res.* **2005**, *1031*, 222−228.
(10) Shemetov, A. A.; Seit-Nebi, A. S.; Gusev, N. B. *J. Neurosci. Res.* **2008**, *86*, 264−269.
(11) Rekas, A.; Jankova, L.; Thorn, D. C.; Cappai, R.; Carver, J. A. *FEBS J.* **2007**, *274* (24), 6290−6305.
(12) Bhattacharyya, J.; Das, K. P. *J. Biol. Chem.* **1999**, *274* (22), 15505−15509.
(13) Thorn, D. C.; Meehan, S.; Sunde, M.; Rekas, A.; Gras, S. L.; MacPhee, C. E.; Dobson, C. M.; Wilson, M.; Carver, J. *Biochemistry* **2005**, *44*, 17027−17036.
(14) Yong, Y. H.; Foegeding, E. A. *J. Agric. Food Chem.* **2010**, *58*, 685−693.
(15) Carrotta, R.; Canale, C.; Diaspro, A.; Trapani, A.; San Biagio, P. L.; Bulone, D. *Biochim. Biophys. Acta* **2012**, *1820* (2), 124−132.
(16) Dickinson, E. *Soft Matter* **2006**, *2*, 642−652.
(17) Marsh, J. A.; Forman-Kay, J. D. *Biophys. J.* **2010**, *98* (10), 2383−2390.
(18) Daughdrill, G. W.; Kashtanov, S.; Stancik, A.; Hill, S. E.; Helms, G.; Muschol, M.; Receveur-Bréchot, V.; Ytreberg, F. M. *Mol. Biol. Syst.* **2012**, *8*, 308−319.
(19) Cabaleiro-Lago, C.; Quinlan-Pluck, F.; Lynch, I.; Lindman, S.; Minogue, A. M.; Thulin, E.; Walsh, D. M.; Dawson, K. A.; Linse, S. *J. Am. Chem. Soc.* **2008**, *130*, 15437−15443.
(20) Kudou, M.; Shiraki, K.; Takagi, M. *Sci. Technol. Adv. Mater.* **2004**, *5* (3), 339−341.
(21) Kudou, M.; Shiraki, K.; Takagi, M. *Protein J.* **2005**, *24* (3), 193−9.
(22) Vetri, V.; Librizzi, F.; Militello, V.; Leone, M. *Eur. Biophys. J.* **2007**, *36* (7), 733−41.
(23) Vetri, V.; Carrotta, R.; Picone, P.; Di Carlo, M.; Militello, V. *Biochim. Biophys. Acta* **2009**, *1804* (1), 173−183.
(24) Carrotta, R.; Vetri, V.; Librizzi, F.; Martorana, V.; Militello, V.; Leone, M. *J. Phys. Chem. B* **2011**, *115* (12), 2691−2698.
(25) Stepanek, P. In *Dynamic Light Scattering: The Method and Some Applications*; Brown, W., Ed.; Clarendon Press: Oxford, U.K., 1993.
(26) Bulone, D.; Giacomazza, D.; Martorana, V.; Newman, J.; San Biagio, P. L. *Phys. Rev. E* **2004**, *69* (4 Pt 1), 041401.
(27) Brown, W. *Light Scattering, Principles and Development*; Oxford University Press: New York, 1996.
(28) Foderà, V.; Groenning, M.; Vetri, V.; Librizzi, F.; Spagnolo, S.; Cornett, C.; Olsen, L.; van de Weert, M.; Leone, M. *J. Phys. Chem. B* **2008**, *112* (47), 15174−81.
(29) Sakono, M.; Motomura, K.; Maruyama, T.; Kamiya, M.; Goto, M. *Biochem. Biophys. Res. Commun.* **2011**, *404*, 494−497.
(30) Dalgleish, D. G.; Corredig, M. *Annu. Rev. Food Sci. Technol.* **2012**, *3*, 449−467.
(31) Enright, M. B.; Leitner, D. M. *Phys. Rev. E* **2005**, *71*, 011912.
(32) de Gennes, P.-G. *Scaling Concepts in Polymer Physics*; Cornell University Press: Ithaca; London, 1979.
(33) Carrotta, R.; Manno, M.; Bulone, D.; Martorana, V.; San Biagio, P. L. *J. Biol. Chem.* **2005**, *280*, 30000−30008.
(34) Zhang, S.; Iwata, K.; Lachenmann, M. J.; Peng, J. W.; Li, S.; Stimson, E. R.; Lu, Y.; Felix, A. M.; Maggio, J. E.; Lee, J. P. *J. Struct. Biol.* **2000**, *130*, 130−141.
(35) Jain, N.; Bhattacharya, M.; Mukhopadhyay, S. *Biophys. J.* **2011**, *101*, 1720−1729.
(36) Corsale, C.; Carrotta, R.; Mangione, M. R.; Vilasi, S.; Provenzano, A.; Cavallaro, G.; Bulone, D.; San Biagio, P. L. *J. Phys: Condens. Matter* **2012**, *24*, 244103.